STRUCTURE, COMPOSITION AND RESIDUAL STRESS ANALYSIS OF TITANIUM NITRIDE THIN FILMS MADE BY DC MAGNETRON SPUTTERING

GUSTAVO MARTINEZ

Department of Mechanical Engineering

APPROVED:

RamanaChintalapalle Ph.D., Chair

Jack Chessa, PhD.

Yirong Lin, Ph.D.

David A. Roberson, Ph.D.

Benjamin C. Flores, Ph.D.
Dean of the Graduate School

Dedicated to my Parents

MICROSTRUCTURE AND MECHANICAL PROPERTIES OF TITANIUM NITRIDE OPTICAL COATINGS MADE BY DC MAGNETRON SPUTTERING

by

GUSTAVO MARTINEZ, B.S.

THESIS

Presented to the Faculty of the Graduate School of

The University of Texas at El Paso

in Partial Fulfillment

of the Requirements

for the Degree of

MASTER OF SCIENCE

Department of Mechanical Engineering

THE UNIVERSITY OF TEXAS AT EL PASO

August 2013

Abstract

Titanium nitride (TiN_x) thin films were grown by DC (Direct Current) magnetron sputtering method onto Si(100) substrates by varying time of deposition to produce films with variable thickness (d_{TiN}) in the range of 20-120 nm. The grown TiN_x films were characterized by studying their structure, composition, and mechanical properties. Nuclear reaction analysis (NRA) combined with Rutherford backscattering spectrometry (RBS) analyses indicate that the grown films were stoichiometric TiN. Grazing incidence X-ray diffraction (GIXRD) measurements indicate that the texturing of the TiN films changes as a function of d_{TiN}. The (111) and (002) peaks appear initially; with increasing d_{TiN}, (111) becomes intense while (002) disappears. Dense, columnar grain structure was evident for the films in scanning electron microscopy analyses. The residual stress d_{TiN}~120 nm was 1.07 GPa in compression while thinner samples exhibit higher values of stress.

Table of Contents

List of Tables

List of Figures

1. Introduction

Titanium nitride (TiN) thin films and coatings have been the subject of intense research due to their exceptional chemical, physical, mechanical and electrical properties, such as a high degree of hardness, chemical stability, high thermal conductivity, resistance to wear and corrosion, chemical inertness and biocompatibility [1-8]. TiN films exhibit a number of properties similar to metals (good electrical conductivity) while retaining characteristics (covalent bonds, hardness, high melting point) found in insulating materials [1-4]. In addition to wear and corrosion, the lustrous color makes TiN coatings useful for decorative applications [9-12]. TiN films serve as metallization materials or diffusion barriers for metal-interconnects in microelectronics [8,13,14]. The optical properties of TiN films make these materials interesting for application in solar cells and plasmonics [11,15]. Currently, there has been a strong interest in TiN nanostructured materials for electronics and energy related technologies [16,17].

The structure, texturing, chemical composition, properties and phenomena of TiN_x films are generally sensitive to the processing parameters employed during fabrication. For instance, the crystal structure and texture of the grown TiN_xlayers are dependent on the ratio of nitrogen to argon in the reactive gas mixture during deposition [11-15,22-43]. Also, it has been reported that the texturing is strongly influenced by coating thickness. Furthermore, TiN_x compounds with a wide range of stoichiometry i.e., x varying from 0.6 to 1.2, were found to be thermodynamically stable. Therefore, simultaneous determination of composition and crystal structure becomes important in order to optimize the processing conditions to obtain stoichiometric films for the aforementioned reasons. The present work was performed on the TiN films produced by direct current (DC) magnetron sputtering onto (100) silicon substrates. The impetus is to understand the

effect of film thickness in the range of 10-120 nm on the microstructure and optical characteristics of the TiN_xnano-crystalline films. While the ultimate goal is to derive a comprehensive understanding of the thickness effects on the optical constants, the present work was focused on understanding the structure, morphology and residual stress of sputter-deposited TiN_x films. The results obtained are presented and discussed in this paper.

2. Experimental details

2.1. Fabrication

Titanium nitride (TiN_x) films were deposited by DC magnetron sputtering method using a Ti-metal target (3" diameter; 0.125" thick) for sputtering. The deposition was made onto well cleaned silicon (Si) (100) substrates. The fabrication conditions employed for TiN films are listed in Table 1.

Table 1. Deposition Parameters

Deposition Parameter	**Set value**
Base Pressure	$5x10^{-8}$Torr
Target	Ti pure (99.99%) (5cm x 0.40 cm)
Substrate	Si (100)
Substrate Temperature	400 ºC
Target substrate distance	8 cm
Target Power	200W
Film thickness	10-120 nm

The deposition was made using a gas mixture containing argon (Ar) and nitrogen (N_2), where Ar and N_2 were the working and reactive gases, respectively. High purity Ar (99.999 %) and N_2 (99.999%) were employed for TiN depositions. A rotary feed through unit holds the substrate to be deposited and turns 2-3 rpm to achieve a more uniform deposition. The chamber was pumped down to a base pressure of $5x10^{-8}$Torr before nitrogen and argon were introduced. The gas mixture was N_2/Ar with a ratio of 25/1. The flow rate of N_2 and Ar were, respectively, 2 and 50 sccm during deposition. A sputtering power of 40 W was initially applied to the Ti-target while

introducing Ar into the chamber to ignite the plasma. Once the plasma was ignited the power was increased to 200 W and high purity N_2 was released into the chamber for reactive deposition. Resistive heather was used below the sample holder to increase the temperature to 400 ^oC for all samples with varying time of deposition to produce TiN films in the thickness range of 10-120 nm. The deposition rate and coating thickness for the set of conditions employed was performed and calibrated in a separate control experiment where the sample was first deposited for 5 min and then examined for thickness. In the control experiments, X-ray reflectivity (XRR) in combination with Rutherford backscattering spectrometry (RBS) was employed to determine thickness (~42 nm). Then, the deposition time was set to produce TiN_x films in the thickness range of 10 nm to 120 nm.

2.2. Characterization

The grown TiN_x films were characterized by evaluating their structure, morphology and residual stress. In order to avoid interference by the substrate and obtain structural information of only the TiN film, grazing incidence X-ray diffraction (GIXRD) was performed. GIXRD measurements were performed using a Bruker D8 Advance X-ray diffractometer. GIXRD patterns were recorded using Cu Kα radiation (λ=1.54056 Å). The X-ray beam was fixed at a grazing incidence of 0.5^o. The scanning was performed in a 2θ range of 15-60^o using the "detector scan" mode. The detector was independently moved to collect the diffraction pattern. From X-ray diffraction data, the interplanar spacing (d_{hkl}) between atomic planes can be determined using the Bragg's relation:

$$2d_{hkl}\mathrm{Sin}\theta = n\lambda \qquad [1]$$

whereλ is wavelength of the X-rays. Titanium nitride exhibits cubic structure in a wide range of compositions. Therefore, the lattice parameter (a) of the grown films can be determined using the relation:

$$a = \mathrm{d}_{\mathrm{hkl}} \sqrt{h^2 + k^2 + l^2} \qquad [2]$$

where (hkl) are Miller indices for the diffraction planes responsible for observed XRD peaks. Surface imaging analysis was performed using scanning electron microscopy (SEM) via a high-performance and high resolution scanning electron microscope (Hitachi S-4800).

The chemical composition of grown TiN_x films as a function of d_{TiN} was determined by Rutherford backscattering spectroscopy (RBS) analysis using a 2.0-MeV tandem electrostatic ion accelerator that provides two stages of acceleration (negative ion acceleration from the source end to the terminal in the middle and positive ion acceleration from the middle to the high-energy end), were the final energy can be controlled depending on the charge state of the ion [44]. The accelerated ions are focused through the high-energy beam line using a magnetic quadrupole and a y-axis electrostatic steerer. The helium ion source used for this analysis was the radio frequency (Alphatross) plasma which accelerated helium ions to the sample to be analyzed in the end station where ion-scattering measurements were performed in the second level using a fixed-position detector at a scattering angle of 150° for RBS spectrometry. The helium beam of 2 MeV ions were used in an incident angle α=7°, the exit angle β=15°, a scattering angle θ=150° and a detector resolution of 20 KeV. RBS results are very accurate with heavy elements such as titanium. However, RBS is not accurate for obtaining the concentration of nitrogen incorporation into the films. For this reason, Nuclear Reaction Analysis (NRA) was also performed in order to have a more accurate composition for lighter elements, specifically nitrogen in the films. NRA is a well suited nuclear method to obtain concentration of lighter elements (such as oxygen and

nitrogen) in a solid thin film. A deuterium (d) beam of 0.94 MeV was used to irradiate the samples. The target elements then undergo a nuclear reaction under resonance conditions for defined resonance energy. This reaction typically produces a nucleus in an excited state which immediately decays, emitting ionizing radiation. In the present case, $^{14}N(d,p)N^{15}$ reaction was employed to probe the nitrogen concentration in the $TiN_x$where this reactions has been used elsewhere to calculate nitrogen content in films [45]. To obtain depth information the initial kinetic energy of the projectile nucleus (which has to exceed the resonance energy) and its stopping power (energy loss per distance traveled) in the sample has to be known. The known "standards" used for composition characterization of N was Si_3N_4(1174±20 Å). The nitrogen concentration was then determined using the following relation:

$$\frac{N_1}{N_S} = \frac{\frac{A_1}{T_1}}{\frac{A_S}{T_S}} \qquad [3]$$

where N represents the element composition be determined, A refers to area under the nitrogen peak in the NRA spectra and T is the thickness of the sample. The subscript 1 refers to the information regarding the sample to be analyzed and subscript S refers to standard information (area and thickness). The uncertainty in determining the N/Ti ratio is less than 5% taking into account both RBS and NRA measurements.

Additional XRD measurements were performed to evaluate the residual stress in the grown films. Stress determination was performed using a modified $sin^2\psi$ technique. In traditional $sin^2\psi$ approach, aspecific diffraction plane is selected and the interplanar spacing is measured from a coupled θ–2θ scan of the specimen at different specimen tilt angle ψ the angle between the diffracting plane normal and the specimen surface normal. Ideally, a high-2θ diffraction peak is chosen to ensure higher sensitivity to strain. Thereafter the residual strain can

be derived from the slope of a linear plot between the fractional change of the plane spacing and $sin^2\psi$ [18]. However, in the case of crystalline films such as TiN only few specific *(hkl)* peaks show up in the XRD pattern. In addition, the diffraction volume in thin films high-2θ diffraction peaks might be too weak to be conveniently measured. These reasons state that traditional $sin^2\psi$ symmetric geometry is unsuitable for calculation of an accurate residual stress analysis. Unlike the traditional $\sin^2\psi$ method, the method proposed employs an asymmetric B-B XRD geometry, with the incident X-ray beam making a grazing angle g with respect to the specimen surface-tilting axis. This method collects diffraction of a particular peak in a single 2θ scan with a fixed low incident-beam angle to the specimen for different ψ angles [18]. TiN characteristic XRD peak corresponding to diffraction from (111) planes is located at 2θ=36.9853°. This particular peak was selected to find the corresponding inter planar distance (d_o) for the corresponding residual stress calculations.

Optimizing thin film properties requires a well-understood relationship between processing parameters, modeling, and model confirmation through novel testing techniques. The calculation of nano-mechanical properties was performed using a Hysitron TI 750 TriboIndenter where indentation and nano scratch testing were used to derive a relation between thicknesses of the films with respect of the mechanical properties. Load-controlled indentation tests were performed on each sample to determine the maximum load that could be applied in the film without penetrating more than 10% of the total film thickness represented in fig. (11).

Tests were performed using a diamond Berkovich tip with a radius of curvature 396 nm to calculate hardness and reduced modulus of each film. Sixteen indents were performed and averaged on each sample, with peak indentation loads in the range of 13-5 μN according to the

thickness of each sample. A representative 2 μm, 2-D topographical in-situ SPM image was obtained on Sample with thickness of 119 nm after a 13 μN load post-indentation, image was captured after nano-indentation test to ensure indents were performed in desired locations. Five load-controlled ramping force scratch tests were also performed on each sample to determine the critical load (P_{crit}) (delamination/breakthrough) of each film and mean roughness the load vs displacement curve can be appreciated in fig (13). The scratch tests were performed using a diamond 90° conical probe with a 100 nm radius of curvature.The peak loads for the ramping force scratch tests were 6000 μN. Each scratch consisted of a 6 μm scratch length and 45-second duration.Similar post-scratch images were captured for each ramping force nanoscratchtest to ensure tests were performed in desired locations, for post-test qualitative surface characterization, and for quantitative nano-scratch depth analysis.

3. Results and discussion

Thickness values of TiN films were primarily probed by the Rutherford backscattering spectrometry (RBS) measurements as a function of variable deposition time. Thickness values obtained using RBS analyses are represented in Fig. 1, where thickness values are plotted against time of deposition. It is evident from Fig 1 that increasing deposition time increases the film thickness. These values were obtained after fitting the experimental RBS curves with SIMNRA [46] program as discussed below. RBS spectra of a representative set of TiN_x films are shown in Fig. 2. The backscattered ions observed were due to various elements, and the positions are indicated by arrows for the experimental spectrum. The scattering from Ti, the heaviest among the elements present either in the film or substrate occurs at higher backscattered energy as shown in RBS curves for TiN_xfilms (Fig. 2). The measured height and width of this peak is related to the concentration and thickness distribution of Ti atoms in the nitride film and serves as calibration check for composition and thickness since known Rutherford scattering cross section and experimental parameters can be used to calculate this height and width [46]. As indicated in the figure, the step edge and peaks due to ion backscattering from Si (substrate) and N atoms (film) are observed at channel number 550 and 1300, respectively. The composition and thickness of the films were determined by simulating the experimental spectrum for the set of experimental conditions.

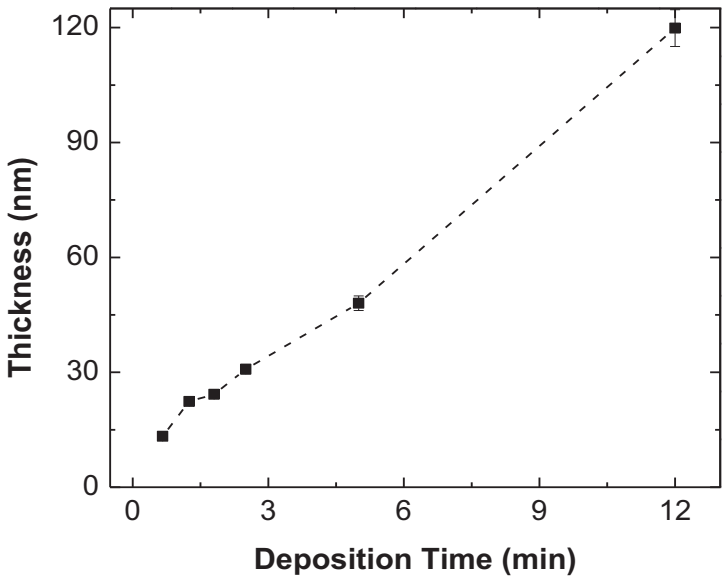

Figure 1. Thickness variation with deposition time of TiN

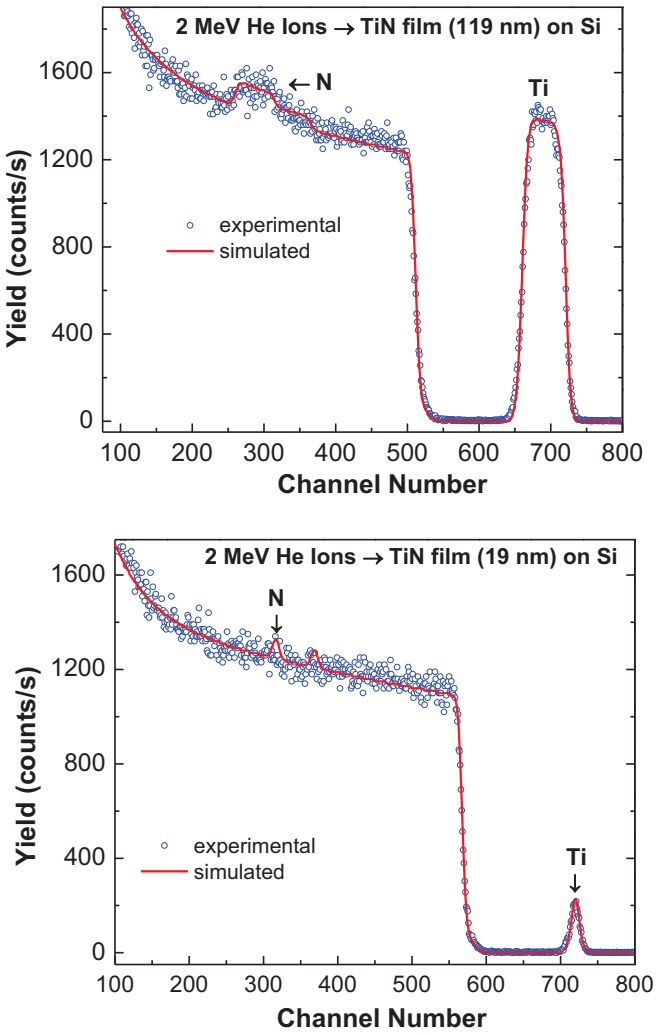

Figure 2.RBS spectra of sample with a thickness of 120 and 19 nm

The procedure utilized to derive the chemical composition of the grown films is also in Fig. 2. The experimental curve (circles) along with the simulation curve (lines) calculated using SIMNRA code is shown. The simulated curve was calculated using SIMNRA code for the fixed set of experimental parameters: (1) incident He^{+} ion energy, (2) integrated charge, (3) energy resolution of the detector, and (4) scattering geometry. RBS data was primarily used to obtain Ti

concentration in the films. The evolution of Ti peak as a function of variable film thickness is shown in Fig. 3. It can be seen that the Ti peak intensity and width increases with film thickness. The intensity and width of the peak accounts for concentration and depth/thickness, respectively, of Ti in the film. To make it clear, the ions scattered from surface, bulk of the film and substrate-film interface are indicated with an arrow in Fig. 3.

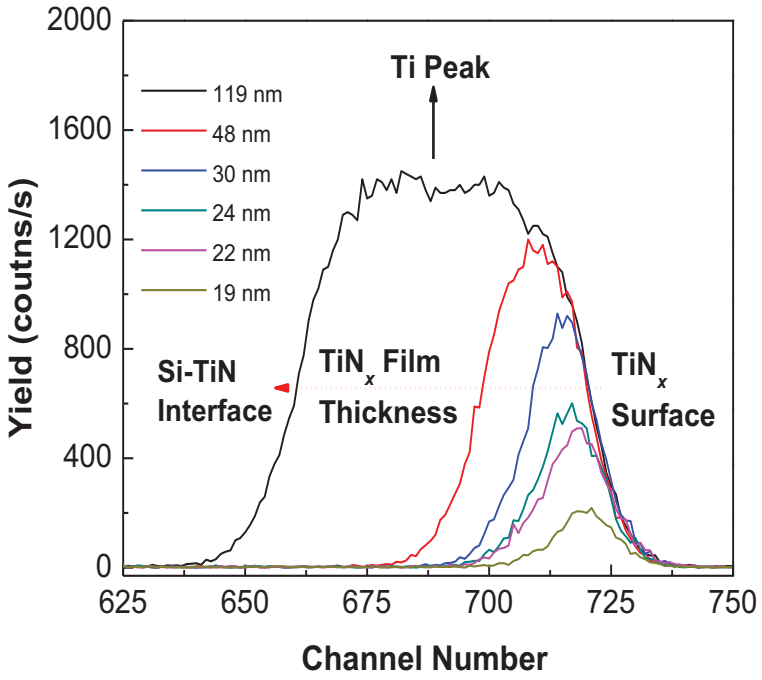

Figure 3.RBS evolution of Titanium peak corresponding to samples in the range of 19-119 nm in thickness

The $^{14}N(d,p)N^{15}$ reaction peak accounting for nitrogen content in the TiN_x films is shown in Fig. 4. It is evident that the intensity and width of this peak increases with increasing film thickness. Two observations that can be noted from Fig. 4 are the following. The nitrogen incorporation into the film readily takes place is the first. Second is the fact that the nitrogen concentration and depth (along thickness) increases with increasing film thickness. Using peak

area the nitrogen concentration is obtained as outlined under experimental section. To understand the evolution of chemical stoichiometry in the films, [Ti]/[N]atomic ratio is calculated using the Ti concentration obtained from RBS and nitrogen concentration obtained from NRA. The accuracy of RBS analysis with heavy metals such as Ti is within the 5% certainty, but with the lighter elements may be greater than 5%. For this reason, combined RBS and NRA data were employed to obtain stoichiometry in the films.

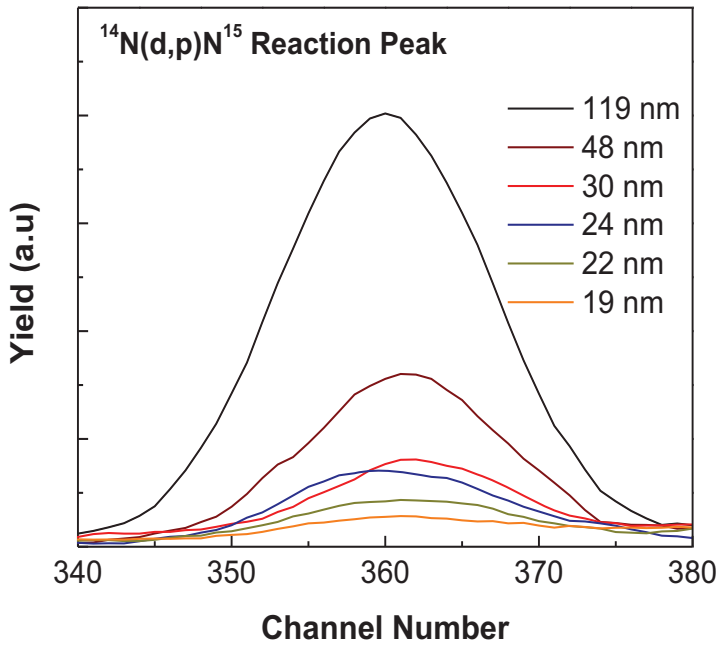

Figure 4. Evolution of 14N(d,p)N15 reaction peak of NRA spectra of 0.94 D beam onto TiN films grown on silicon with increasing thickness

The results obtained are shown in Fig. 5. The relatively thicker films (>20 nm) films are found to be stoichiometric with a [Ti]/[N] ratio in the range of 1.04-0.97. However, for the set of relatively thinner films, the stoichiometry is found to be deviating with a Ti metal deficiency. [Ti]/[N] ratio for these films is found to be of ~0.6. This cannot be interpreted that the thinner

films grown were non-stoichiometric because of the fact that NRA is not accurate and has a limitation with probing depth. NRA will not provide accurate information for films < 50 nm. Therefore, for the set of experimental conditions employed, we believe that films were stoichiometric.

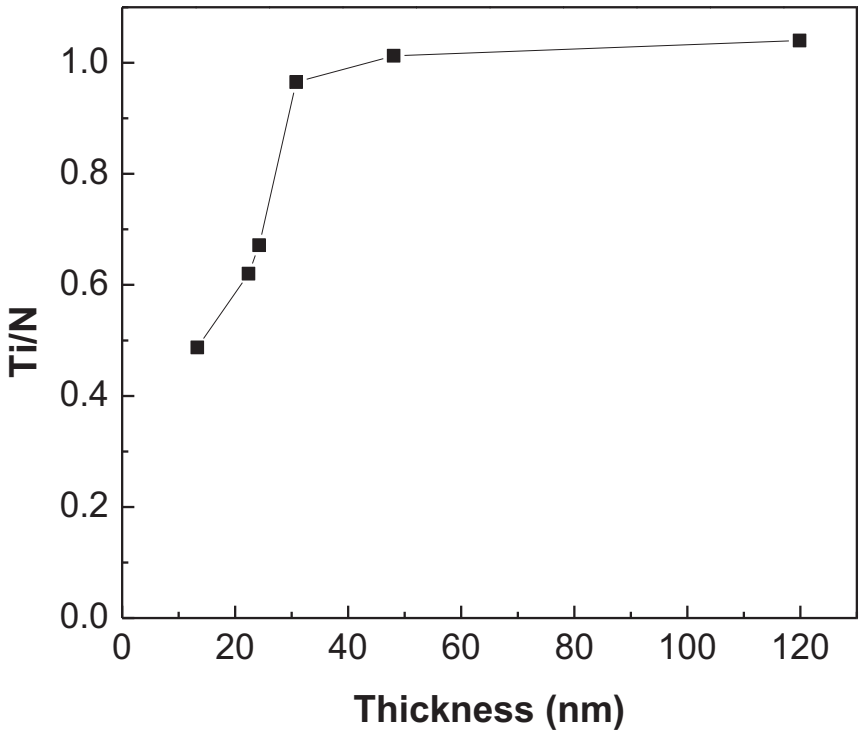

Figure 5. [Ti]/[N] stoichiometry ratios with respect to increasing thickness

The XRD patterns obtained for TiN films with variable thickness are presented in Fig. 6. The XRD patterns exhibit peaks corresponding to cubic TiN. The peak located at 2θ~36.9° corresponds to diffraction from (111) planes. It can be observed that the broadness of this particular peak increases at the same time the intensity of the peak decreases as the thickness of the film decreases. For TiN films with a thickness of 24 nm, the XRD data indicate the onset of a

peak corresponding to diffraction from (111) planes of cubic-TiN. For continued deposition or increasing thickness of TiN films, onset of (002) peak 2θ=42.7° is noted. A minimum thickness to obtain (111) texturing is ~22-25 nm for this particular set of growth conditions and as the thickness of the film increases the dominance of the (111) plane becomes evident.

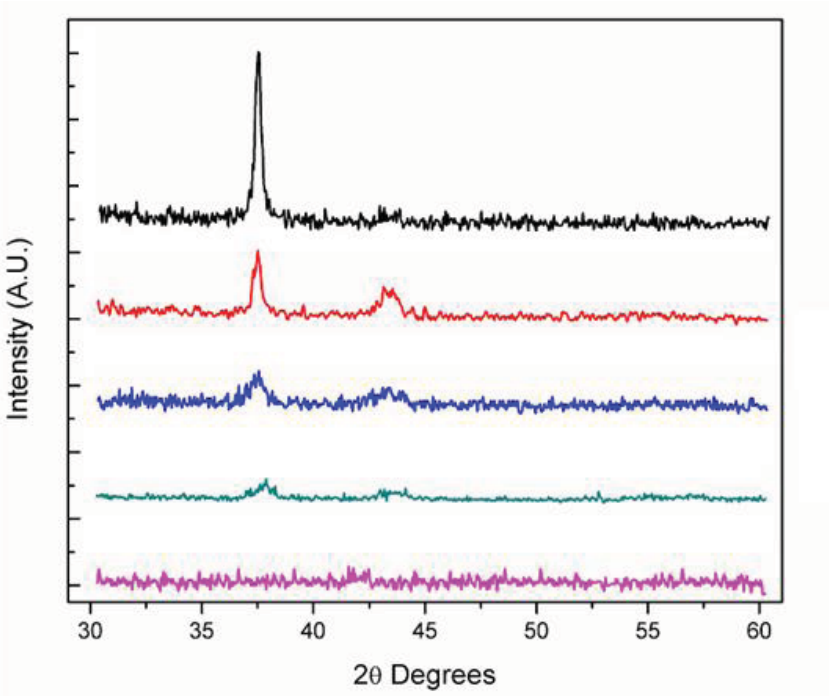

Figure 6. XRD patterns of TiN coatings with variable thickness

The evolution of (111) peak with film thickness is shown in Fig. 7. As the film thickness increases the (111) peak counts increase (Fig. 7) indicating of an increase of the average crystallite-size and preferred orientation of the film along (111). At the same time the intensity of the peak corresponding to (002) decreases until it finally disappears at d_{TiN}~48-120 nm. TiN_x sample with d_{TiN}=120 nm exhibits the highest intensity and (111) orientation. It is evident that when TiN is found in (111) orientation the intensity of the peaks found stronger compared to the

intensity found when the thickness decreases, this also the case for the broadness of the peak that becomes wider at the base as thickness decreases.

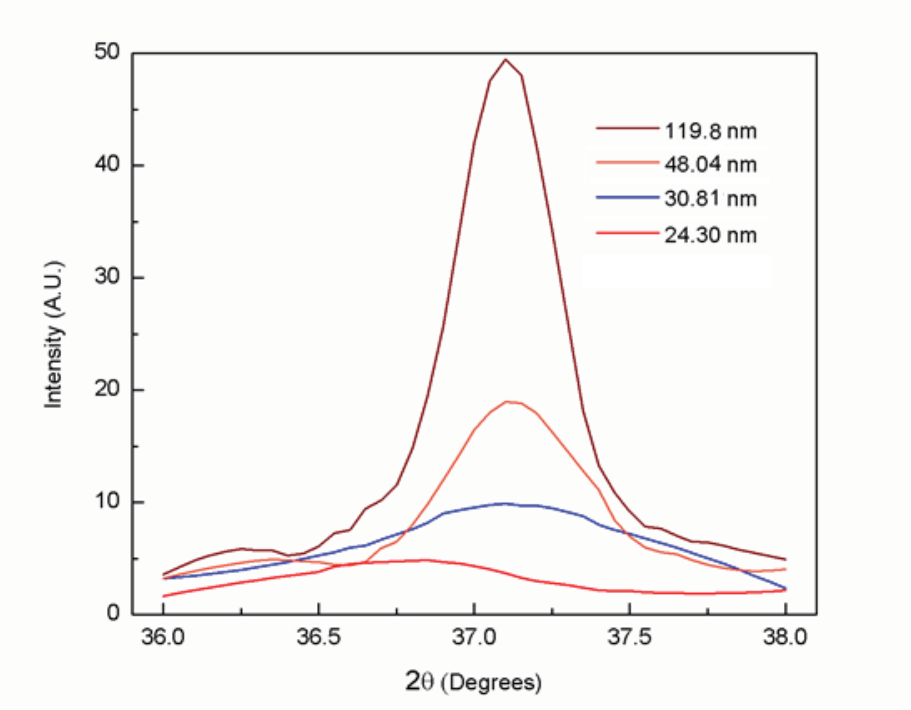

Figure 7. Evolution in high resolution GIXRD scan of the peak located at 2Θ=37

This behavior reflected by intensity and broadness of peaks is also reflected on the grain size in SEM images shown in Fig. 8. The texture change can be mostly identified with the increase in size and shape of the grains with increasing thickness. The samples with a thickness of anything less than 22 nm in thickness will not show any grain formation. It is evident (Fig. 8) that the samples with a thickness of 24 nm or higher present circular shape grains. With increasing deposition time, the shape changes to a triangular like shape. The triangular shape and grain size will become more defined and bigger as the (111) orientation in the film becomes dominant. The samples demonstrate columnar structure growth as ids depicted in Fig. 9.

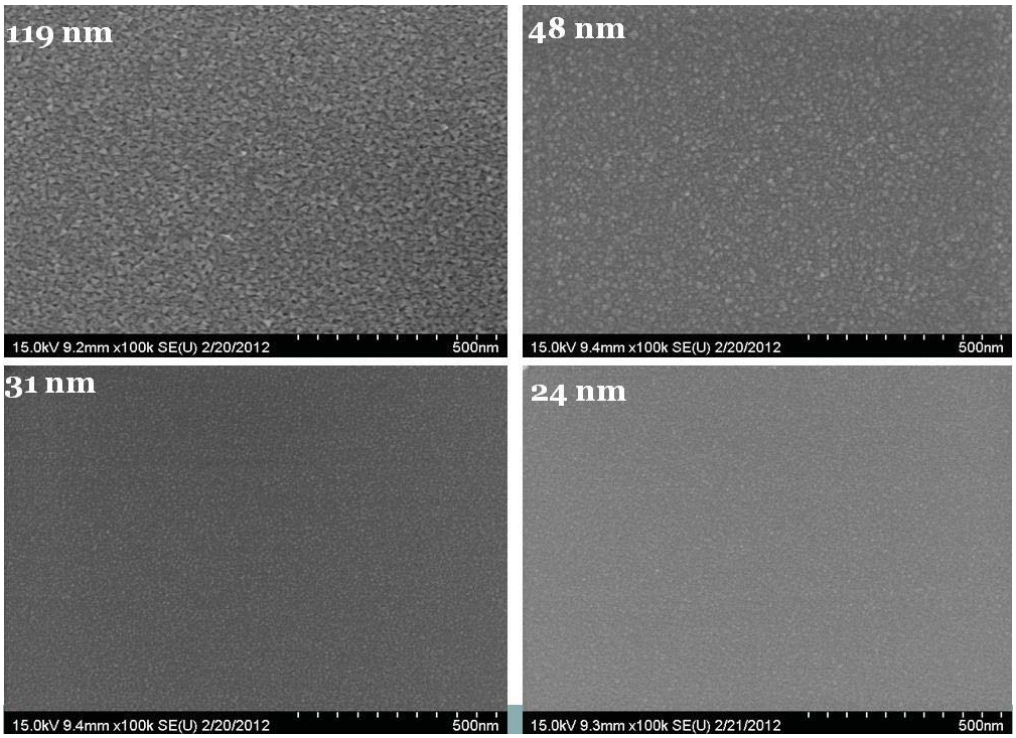

Figure 8.SEM images for TiN coatings surface morphology at different thickness values: a) ~119 nm; b) ~48 nm; c) ~31 nm; d) ~24 nm

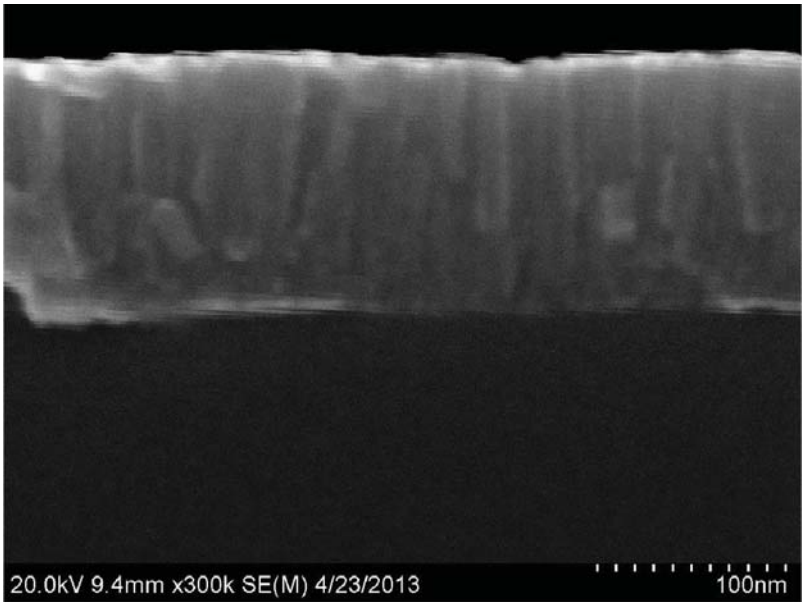

Figure 9.SEM image cross section corresponding to sample with a thickness of 119 nm

For both substrates the positions of (111) and (002) Bragg's reflections are found to be systematically shifting to higher 2θ angles as the thickness of the film increases. Meaning that the out of plane interplanar spacing is increasing as the thickness increases and for this reason the presence of compressive stress is also evident and decreasing as the thickness of the film increases. This phenomena can be better appreciated at Fig. 7 where the evolution of the (111) peak located at 2Θ = 37° is observed in high resolution GIXRD scan. Using grazing incidence XRD and a modified $\sin^2\psi$ method in a range of ψ values from -10° to 10° the strain/stress of TiN films was calculated. It can be clearly appreciated that the (111) peaks were shifting towards higher angles but, using this method it was found that the global stress in all samples was in compressive state. with the values -1.07 for the sample with a thickness of 119 nm giving the least amount of stress in the thickest samples, as for the sample with a thickness of 48 nm the global stress was higher at -3.15 Gpa. Similar values of stress were obtained by the work of Abadias [23].The use of a stress analysis enabled us to determine the behavior of stress with increasing thickness and substrate used for growing TiN films. Figure (10) depicts the samples with a thickness of 119 and 48.04. Mahieu et al. [47] also noted that as the samples become thinner the state of stress increases represented in the graph as steeper trend lines. The reason for this is that at thickness lower that 119 nm other orientations of TiN manifest and increase the state of stress in the film.

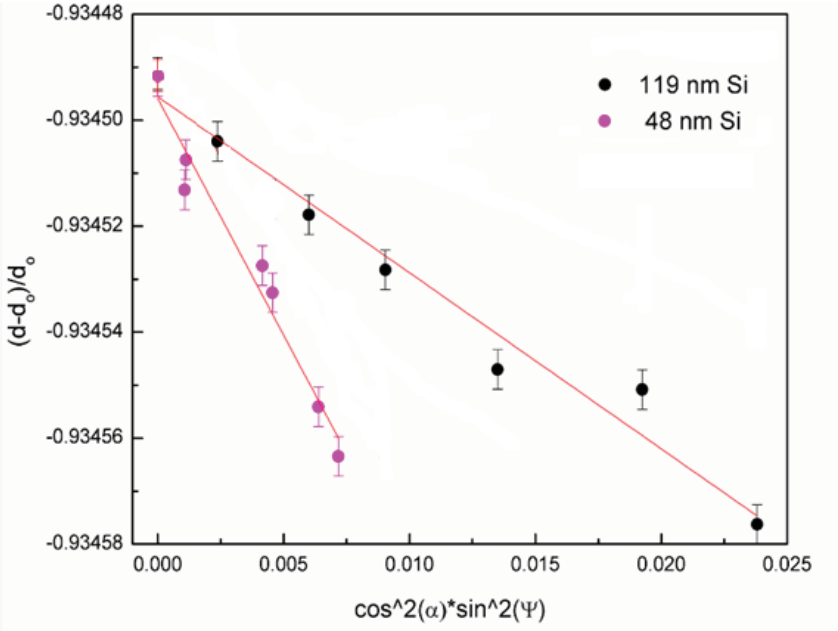

Figure 10.Residual stress plot corresponding samples with a thickness 119 -48 nm grown on Si

To obtain the hardness (H) and elastic modulus (E) of the TiN thin films grown at varied deposition times the nano-indentation measurements were conducted, the results are shown in table 2. Mechanical properties could not be obtained for samples with less thickness of 31nmthis because the TiN film was extremely thin and exceeded the limits of the nano indentation machine. The plot depicting load vs displacement can be appreciated in fig.(12) were it can be observed a typical behavior in this type of analysis. From table 2 it can be observed that as the thickness of the TiN film increases the hardness and the elastic modulus also increase, this as previously demonstrated by G. Abadias [23].

Table 2. Mechanical testing results from nano-indentation and nano-scratch.

Sample thickness (nm)	Er (GPa)	H (GPa)	Mean Roughness(nm)	P_{crit} (μN)
120	125	6.24	0.7	2342
48	120	6.30	1.2	974
31	114	5.82	1.2	728

This result agrees well with research reports [50] showing that TiN thin film hardness increases with an increase in the (111) texture coefficient. In the present research the sample deposition time increases and the same time the (111) plane orientation intensity also does eventually becoming the dominant plane. The hardness and the elastic modulus are shown to be the maximum values of 6.30 and 125 GPa, respectively. Compared this values with those reported in literature for hardness and modulus of elasticity in the range of 5-60 and 100-400 GPa respectively [48], it can be observed that the obtained values of this research fall in the lower range when compared to literature values. This behavior is a result that film thickness has a direct proportional impact on the film modulus of elasticity and hardness [49-50]. The TiN thin film with thickness of 120nm also shows the highest texture coefficient value. As a result, the hardness and elastic modulus of the as grown TiN thin film depended on the degree of (111) preferential orientation.

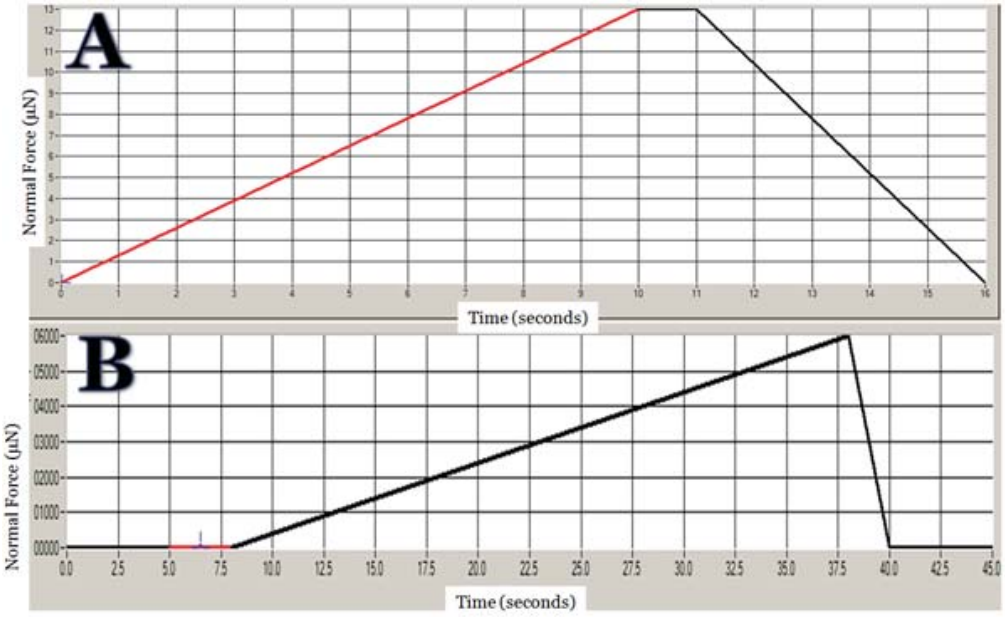

Figure 11.A) load controlled ramping force plot. B) Load controlled ramping force loading and unloading with respect to time

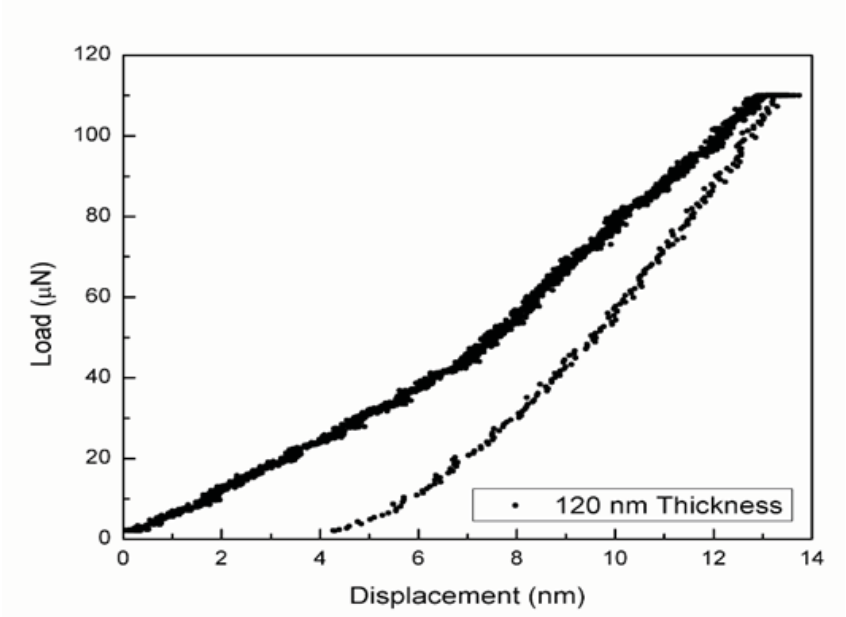

Figure 12. Load VS displacement nano-indentation curve of sample corresponding of 119 nm in thickness

The nano-scratch test results can be appreciated in figure (13) were it can be observed the force applied for the experiment and how the critical load P_{crit} is identified in the plot. The P_{crit} fallows the same behavior observed for the modulus of elasticity and hardness were the thickest sample with the dominant (111) plane orientation derives the best results measuring 2342μN force required for delamination of the film-substrate interface.

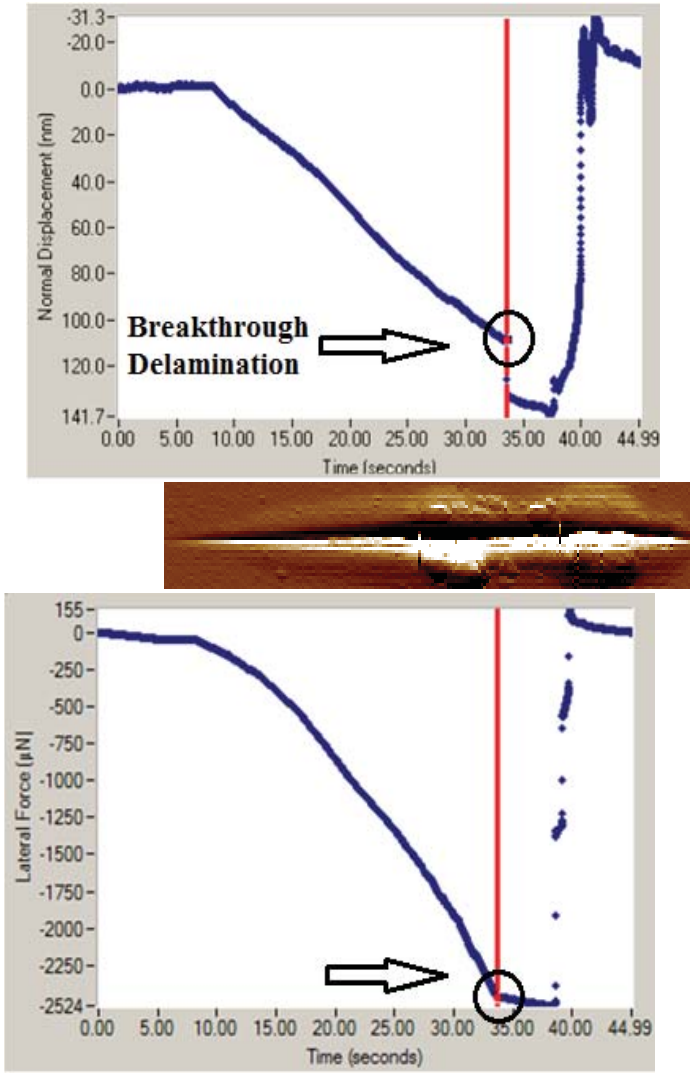

Figure 13. A) Normal displacement VS time curve when nano-scratch testing is performed. B) 2-D topographical in-situ SPM image of the nano- scratch performed on sample with 119 nm in thickness. C) Lateral force VS time curve of nano-scratch testing

4. Conclusions

TiN films with variable thickness in the range of 20-120 nm were fabricated employing DC sputtering. The effect of film thickness on the structure and residual stress evolution was examined in detail. XRD analyses indicate that nano-crystalline TiN films coatings exhibit the (111) preferred orientation. A compressive stress across the substrate-coating interface exists for the films grown on Si while the magnitude is higher for the thinner samples. The chemical stoichiometry of the grown films was studied using a combined RBS and NRA approach. The relatively thicker films (>20 nm) films were stoichiometric with a [Ti]/[N] ratio in the range of 1.04-0.97.

References

1. J. E. Sundgren, Thin Solid Films 128, 21 (1985).
2. H. Ljungcrantz, M. Oden, L. Hultman, J. E. Greene, and J. E. Sundgren, J. Appl. Phys. 80, 6725 (1996).
3. H. E. Rebenne , D. G. Bhat, Surf. Coat. Technol. 63, 1 (1994).
4. W. J. Chou, G. P. Yu, J. H. Huang, Surf. Coat. Technol. 149, 7 (2002)
5. K. D. Preston, G. H. Haertling, Integrated Ferroelectrics, Volume 1, 1, 1992.
6. H. Onoda, M. Kageyama, K. Hashimoto, J. Appl. Phys. 77 (1995) 885.
7. D.B. Knorr, S.M. Merchant, M.A. Biberger, J. Vac. Sci. Technol., B 16(1998) 2734.
8. J.S. Chun, I. Petrov, J.E. Greene, J. Appl. Phys. 86, 3633 (1999).
9. J. Chu, X. Ma, D. Yang, D. Que, Semiconductor Technology, 154(2001)
10. S. Kadlec, J. Musil, J. Vyskcil, Surf. Coat. Technol. 54/55, 249 (1992).
11. N. Kalfagiannis, S. Logothetidis, Rev. Adv. Mater. Sci.15, 167 (2001).
12. S. Niyomsoan, W. Grant, D.L. Olson, B. Mishra, Thin Solid Films 415, 187 (2002).
13. L. Gao, J. Gsto¨ttner, R. Emling, M. Balden, Ch. Linsmeier, A. Wiltner, W. Hansch, D. Schmitt-Landsiedel, Microelectron. Eng. 76, 76 (2004).
14. M. Moriyama, T. Kawazoe, M. Tanaka, M. Murakami, Thin Solid Films 416, 136 (2002).
15. G.M. Matnenoglou, S. Logothetidis, and S. Kassavetis, Thin Solid Films 511–512, 453 (2006).
16. S. Dong, X. Chen, L. Gu, X. Zhou, H. Xu, H. Wang, Z. Liu, P. Han, J. Yao, L. Wang, G. Cui, and L. Chen, ACS Appl. Mater. Interfaces 3, 93 (2011).
17. L.P.B. Lima, J.A. Diniz, I. Doi, J. Godoy Fo, Microelectronic Engineering. 92, 86 (2012).

18. C.-H. Maa, J.-H. Huangb, Haydn Chena, Thin Solid Films, 418 73–7873–78 (2002).

19. I. P. Jain, G. Agarwal, Surface Science Reports, Vol 66, 3-4 (2011)

20. M. Kobayashi and Y. Doi, Thin Solid Films 54, 67 (1978)

21. W.F. Wu, K.C. Tsai, C.G. Chao, J.C. Chen, K.L. Ou,J. Electron. Mater. 446, 184 (2004).

22. D. Gall, S. Kodambaka, M.A. Wall, I. Petrov, J.E.Greene, J. Appl. Phys. 93, 9086 (2003).

23. G. Abadias, Surf. Coat. Technol. 202, 2223 (2008).

24. R. Banerjee, R. Chandra, P. Ayyub, Thin Solid Films 405, 64 (2002).

25. C. Ziebert, S. Ulrich, J. Vac. Sci. Technol. A 24, 554(2006).

26. I. Petrov, P.B. Barna, L. Hultman, J.E. Greene, J. Vac.Sci. Technol. A 21, S117 (2003).

27. W.J. Meng, T.J. Curtis, J. Electron. Mater. 515, 1229(2006).

28. G. Abadias, Y.Y. Tse, Ph. Guerin, V. Pelosin, J. Appl.Phys. 99, 113519 (2006).

29. H. Wang, A. Gupta, A. Tiwari, X. Zhang, J. Narayan,J. Electron. Mater. 32, 994 (2003).

30. T.Q. Li, S. Noda, H. Komiyama, T. Yamamoto, Y.Ikuhara, J. Vac. Sci. Technol. A 21, 1717 (2003).

31. Y.H. Cheng, B.K. Tay, J. Cryst. Growth 252, 257 (2003).

32. S. Piscanec, L.C. Ciacchi, E. Vesselli, G. Comelli, O.Sbaizero, S. Meriani, A. De Vita, Acta Mater. 52, 1237(2004).

33. J. H. Je, D. Y. Noh, H. K. Kim, K. S. Liang, J. Appl. Phys. 81, 6126 (1997)

34. M. J. Williamson, D. N. Dunn, R. Hull, S. Kodambaka, I. Petrov, J. E. Greene, Appl. Phys. Lett. 78, 2223 (2001)

35. T. Q. Li, S. Noda, Y. Tsuji, T. Ohsawa, H. Komiyama, J. Vac. Sci. Technol. A 20, 583 (2002).

36. T. Q. Li, S. Noda, H. Komiyama, T. Yamamoto, Y. Ikuhara, J. Vac. Sci. Technol. A 21, 1717 (2003)

37. J. S. Chun, I. Petrov, J. E. Greene, J. Appl. Phys. 86, 3633 (1999).

38. J. Pelleg, L. Z. Zevin, S. Lungo, N. Croitoru, Thin Solid Films 197, 117 (1991)

39. J. P. Zhao, X. Wang, Z. Y. Chen, S. Q. Yang, T. S. Shi, X. H. Liu, J. Phys. D 30, 5 (1997)

40. U. C. Oh, J. H. Je, J. Appl. Phys. 74, 1692 (1993).

41. U. C. Oh, J. H. Je, J. Y. Lee, J. Mater. Res. 13, 1225 (1998)

42. S. H. Lim, D. G. McCulloch, M. M. M. Bilek, D. R. McKenzie, J. Appl. Phys. 93, 4283 (2003).

43. C.V Ramana, S. White, N. Esparza, V. Rangel,A.L. Campbell, Journal of Electronic Materials, Vol. 41, No. 11, (2012)

44. I.P. Jain ,GarimaAgarwal, Surface Science Reports, 66,77–172 (2011).

45. H.-T. Tang, H-T, W.N. Lennard, M. ZinkeAllmang, I.V. Mitchell, L.C. Feldman, M.L. Green, D. Brasen, Appl. Phys. Lett. 64, 3473 (1994)

46. Mayer, Matej. SIMNRA user's guide. No. IPP 9/113. Max-Planck-Inst. fürPlasmaphysik, (1997).

47. S. Mahieu, P. Ghekiere, G. De Winter, S. Heirwegh, D. Delpha, R. De Gryse, O.I. Lebedev, G. Van Tendeloo, J. Cryst. Growth 279 (2005).

48. W.J. Chou, G.P.Yu, J.H. Huang, Surf. Coat, Technol. 149 7-13 (2002).

49. Soo Ho Kima,b, Hoon Parka, KwangHoonLeea, Seung Hyun Jeea, Dong-JooKimb, Young SooYoonc, HeeBaikChae. Journal of Ceramic Processing Research. Vol. 10, 49-53 (2009).

50. Jeffrey Schirer, Julia Nowak. Department of Chemistry, Kanazawa Institute of Technology, Japan

Curriculum Vita

Gustavo Martinez was born on June16th, 1987 in El Paso, USA. The second son of Adolfo Martinez and Alejandra Escarcega, he graduated from University of Texas at El Paso with abachelor's degree in Mechanical Engineering. He stayed at University of Texas at El Paso to pursue itsmaster's degree in Mechanical Engineering. During his master's, he worked as a research assistant in the department of mechanical engineering. He is a member of the Center for Space Exploration Technology Research cSETR center in the department of Mechanical Engineering. He attended numerous conferences to present the work in this thesis. He also devoted two summers as an intern graduate student in the Pacific Northwest National Laboratory (PNNL). In summer 2013, he graduated with a Master of Science degreein Mechanical Engineering and proceeded further to pursue his Ph.D in the ESE program at UTEP.